Iterative Learning Observer-Based Composite SOSM Control for PMSM Speed Regulation Problem With Mismatched Disturbances

Chang Cheng, Lu Liu, and Shihong Ding, *Senior Member, IEEE*

***Abstract*—Aiming at the speed regulation problem of the permanent magnet synchronous motor (PMSM) in the presence of torque ripple and external disturbance, a composite control algorithm is proposed by combining an iterative learning control based on disturbance observer (ILC-DOB) with a second-order sliding-mode (SOSM) control scheme, which can improve the robustness and the ability of torque ripple suppression for the PMSM speed regulation system. First, the mathematical model of the PMSM is constructed and then transformed into an SOSM dynamics with mismatched disturbance. Second, a novel ILC-DOB is introduced to estimate the mismatched disturbance containing periodic torque ripple. Finally, a composite SOSM control algorithm with state feedback and feedforward compensation is constructed. Consequently, the robustness of the PMSM system is improved, and the torque ripple is also minimized. On this basis, the performance of the PMSM speed regulation system is improved. Through experimental results, the effectiveness of the proposed composite control algorithm is verified.**

***Index Terms*—Disturbance observer, iterative learning control (ILC), mismatched disturbance, permanent magnet synchronous motor (PMSM), second-order sliding mode (SOSM).**

I. Introduction

FOLLOWING the development of power electronics technology [1], [2], the permanent magnet synchronous motor (PMSM) has become the core power unit in aerospace, rail transportation, new energy, and other fields due to its remarkable advantages, such as high power density, high torque density, and wide speed regulation range [3], [4]. Generally speaking, the magnetic field-oriented control (FOC) is widely used in the PMSM system for its high control efficiency and control accuracy, which is structured as a series control structure with a speed loop and two current loops, where the conventional PI control technique is still popular because of its simple implementation [5]. Unfortunately, the actual PMSM system contains massive internal or external disturbance and uncertainty [6], [7], which usually consists of torque ripple, unmodeled dynamic, parameter variation, frictional force, load disturbance, etc. Under these circumstances, the traditional linear control methods represented by PI control are difficult to possess satisfactory robustness.

To this end, several nonlinear control methods are employed in the PMSM to improve its steady-state and transient performance, such as feedback linearization control (FLC) [8], [9], deadbeat control [10], [11], model predictive control (MPC) [12], [13], fuzzy logic control [14], [15], neural network control [16], and sliding-mode control (SMC) [17], [18]. Among them, the FLC scheme has satisfactory speed tracking performance without parameter variation of the PMSM model [8], [9]. However, it cannot keep acceptable transient performance since its fixed gain cannot vary with the change of working conditions. Next, the deadbeat control can realize the tracking goal without overshooting and the fast dynamic response of the system [10], [11], while it requires high precision of the PMSM mathematical model. In addition, the MPC method is simple in the design process and can deal with various constraints on spatial state variables [12], [13], however, it not only requires high model accuracy but also is computationally intensive to solve optimization problems. It is obvious that all the abovementioned three nonlinear control methods require an accurate system model to overcome parameter variation problems. On the contrary, the fuzzy logic control can handle the uncertainties and nonlinearities of the PMSM system without an accurate mathematical model [14], [15], while the rough fuzzy rules will degrade steady-state and dynamic performance. In [16], the neural network control is utilized to approximate complex nonlinear relationships for strong robustness and fault tolerance. However, there are several crucial issues such as training set problem, normalization, and computational burden need to be further addressed. Compared with the abovementioned control strategies, the SMC method has been receiving widespread attention due to its insensitivity to model error, parameter variation, and external disturbance. Therefore, it has been successfully applied to the PMSM system [17], [18]. Unfortunately, the SMC has two shortcomings. First, the chattering problem caused by discontinuous high-frequency switching signals affects the control performance of the system. Second,

Manuscript received 9 November 2023; revised 4 February 2024 and 31 March 2024; accepted 4 May 2024. Date of publication 13 May 2024; date of current version 20 June 2024. This work was supported in part by the National Natural Science Foundation of China under Grant 62103170, Grant 61973142, and Grant 62373170, in part by the Natural Science Foundation of Jiangsu Province under Grant BK20210745, in part by the Jiangsu Province and Education Ministry Co-sponsored Synergistic Innovation Center of Modern Agricultural Equipment under Grant XTCX2015. Recommended for publication by Associate Editor K.-B. Park. *(Corresponding author: Shihong Ding.)*

The authors are with the School of Electrical and Information Engineering, Jiangsu University, Zhenjiang, Jiangsu 212013, China (e-mail: chengchang@stmail.ujs.edu.cn; liulu2021@ujs.edu.cn; dsh@ujs.edu.cn).

Color versions of one or more figures in this article are available at https://doi.org/10.1109/TPEL.2024.3398775.

Digital Object Identifier 10.1109/TPEL.2024.3398775

the traditional first-order SMC can only be applied to the systems with a relative degree of one.

To address the aforementioned disadvantages, the concept of high-order sliding mode was systematically introduced for the first time in [19], where the relative order limitation and the chattering problem are solved without losing the strong robustness of the traditional SMC method [20]. On this basis, various second-order sliding-mode (SOSM) algorithms have been proposed and applied to the PMSM system in recent decades [21], such as twisting algorithm [22], suboptimal algorithm [23], super-twisting algorithm [24], quasi-continuous algorithm [25], and relay polynomial algorithm [26]. Among these algorithms, the relay polynomial algorithm gives a more concise structure to construct the SOSM controller with the help of the backstepping-like technique [27].

It should be pointed out that the concept of mismatched terms can be introduced in the relay polynomial algorithm, while the traditional SOSM dynamics is obtained by taking the second-order derivative directly on the sliding variable. Obviously, the traditional SOSM method brings all the information of the system into the control channel, where the uncertainties are significantly increased [28], [29]. Therefore, introducing a mismatched uncertainty term could effectively reduce the uncertainties in the control channel. In this situation, the uncertainties can be suppressed with a lower control gain, which results in the chattering problem being weakened [30]. Moreover, in the actual PMSM system, there are often some external disturbances in the mismatched channel, which cannot be handled by the relay polynomial algorithm directly. Based on this, the disturbance observation (DOB) technique is considered to deal with the nonvanishing mismatched disturbance.

The DOB technique has been widely applied in the speed regulation problem of the PMSM to accurately estimate and compensate for disturbance [31]. In [32], an improved robustness observer was applied to enhance the PMSM system robustness. Moreover, an extended-state observer was used to estimate the lumped disturbance in the absence of exact information on the speed loop [33]. It should be noted that the estimated values of the abovementioned DOB are time-varying. This means that the periodic torque ripple of the PMSM system during operation could not be exactly estimated since it varies periodically with the rotor position [34], which will degrade the drive performance of the PMSM system, particularly at a low speed. To enhance the observation capability of the DOB for periodic disturbance, an iterative learning control based on high-gain DOB (ILC-DOB) was proposed in [35]. The iterative learning control (ILC) is a data-driven control method that can optimize the control signal of the current iteration cycle by learning information from the previous iteration cycle continuously [36]. In addition, the ILC and SMC are combined to minimize the torque ripple of the PMSM [37]. In [38], an improved iterative learning direct torque control is proposed for torque ripple minimization. In [39], an innovative ILC law is used to reduce the steady-state error caused by a load disturbance torque. Consequently, the ILC has an ideal suppression capability for the periodic torque ripple.

Inspired by the abovementioned discussion, for the speed regulation problem of the PMSM system, an iterative learning observer-based composite SOSM algorithm is proposed in the absence of the ripple. First, the relay polynomial algorithm is adopted for the controller design of the PMSM system with mismatched disturbance. Second, a novel ILC-DOB is introduced to improve the suppression capability of the DOB for the torque ripple. Finally, a novel composite SOSM control is constructed by combining the ILC-DOB with the relay polynomial algorithm, which can duly handle the ripple problem and then weaken the chattering problem. The main contributions of this article mainly include the following.

1) Different from the traditional SOSM controller design method, a composite SOSM controller for the PMSM system is designed by combining a simpler relay polynomial algorithm with the DOB technique.
2) Compared with the traditional SOSM algorithm, the proposed composite SOSM algorithm can deal with the mismatched disturbance, which reduces the chattering problem and also ensures the robustness.
3) Distinguished from the traditional DOB, a new ILC-DOB is introduced to minimize the periodic torque ripple of the PMSM.

The rest of this article is organized as follows. In Section II, the mathematical model of the PMSM is given and the components of the torque ripple are analyzed. In Section III, the mathematical model of the PMSM is first transformed into SOSM dynamics with mismatched disturbance. Next, a novel ILC-DOB is designed based on the SOSM system. Finally, a composite SOSM controller is designed and its stability is analyzed. In Section IV, the experiments are conducted to verify the proposed control method. Finally, Section V concludes this article.

Throughout this article, $\lfloor x \rceil^a$ denotes $|x|^a \operatorname{sign}(x)$ with $a > 0$.

II. System Modeling and Analysis of Torque Ripples

The mathematical model of the surface-mounted PMSM is established, on the basis of which the torque ripple analysis is carried out.

A. Mathematical Model of PMSM

For the simplicity of analysis, the saturations of iron core, eddy current, and hysteresis loss are ignored. The voltage equations for the stator dq axis of the PMSM in synchronous rotating coordinate systems can be formulated as

$$\begin{cases} u_d = Ri_d + L_d \frac{di_d}{dt} - p_n w L_q i_q \\ u_q = Ri_q + L_q \frac{di_q}{dt} + p_n w L_d i_d + p_n w \psi_f \end{cases} \tag{1}$$

where u_d and u_q are the stator voltages of the dq axis, i_d and i_q are the stator currents of the dq axis, L_d and L_q are the inductances of the dq axis, R is the stator resistance, p_n is the number of pole pairs, w is the mechanical angular velocity, and ψ_f is the rotor flux linkage. It should be further considered that the surface-mounted PMSM with a salient rate of one, which implies $L_d = L_q$.

The FOC scheme is adopted for the PMSM system, which means that the d-axis current should be zero. The dynamic

equation of the motor can be formulated as

$$J\frac{dw}{dt} = T_e - Bw - T_L \tag{2}$$

where J is the inertia, B is the frictional coefficient, T_L is the load torque, T_e is the electromagnetic torque, which is expressed as

$$T_e = \frac{3}{2}p_n i_q \left[i_d \left(L_d - L_q\right) + \psi_f\right] = \frac{3}{2}p_n \psi_f i_q. \tag{3}$$

B. Analysis of Torque Ripples

In the presence of torque ripples during PMSM operation, the electromagnetic torque (3) can be rewritten as

$$T_e = \frac{3}{2}p_n \left[\psi_f + \sum_{l=1}^{\infty} \psi_{6l} \cos\left(6l\theta_e\right)\right] \cdot \left(i_1 + i_2 + i_q\right) + T_c \tag{4}$$

where ψ_f and ψ_{6l} are the rotor PM flux linkage and 6 lth-order harmonic amplitude, θ_e is the electrical angle of the PMSM, i_1 and i_2 denote the current measurement errors generated by current offset and scaling separately, and T_c denotes the cogging torque. Generally speaking, the torque ripple is generated by flux harmonic, cogging torque, and current measurement error, which will cause the speed fluctuation, noise, and mechanical vibration in the motor [34]. According to the abovementioned analysis, the torque ripples in (4) could be expressed as

$$\begin{cases} i_1 = \frac{2}{\sqrt{3}}\sqrt{\Delta i_a^2 + \Delta i_b^2 + \Delta i_a \Delta i_b} \cdot \cos\left(\theta_e + \xi\right) \\ i_2 = \frac{I}{\sqrt{3}}\left(\frac{f_a - f_b}{f_a f_b}\right)\left[\cos\left(2\theta_e + \frac{\pi}{3}\right) + 0.5\right] \\ T_c = \sum_{l=1}^{\infty} T_{\text{cl}} \sin\left(lC_{\min}\theta_e\right) \end{cases} \tag{5}$$

where Δi_a and Δi_b are the dc offsets of a-phase and b-phase stator current detection, ξ is a constant angular associated with Δi_a and Δi_b, I denotes the amplitude of the phase current, f_a and f_b are the scaling factors of i_a and i_b, T_{cl} denotes the harmonic amplitude of the lth cogging torque, and $C_{\min}$ denotes the smallest common multiple within the number of the PMSM cogging and pole pairs.

Obviously, it can be known from (4) that the flux harmonic is mainly composed of the sixth and 12th periodic harmonics generated by the nonsinusoidal magnetic chain distribution. According to (5), the current offset error could generate torque oscillation at the fundamental frequency, and the current scaling error will generate torque oscillation at twice the fundamental frequency.

Consequently, the electromagnetic torque consists primarily of the dc component as well as the first, second, sixth, and 12th harmonic components, and the torque ripple varies periodically during the running of the motor. Therefore, (4) can be simplified as

$$T_e = \frac{3}{2}p_n \psi_f i_q + T_{\text{tr}} = \frac{3}{2}p_n \psi_f i_q + \sum_{l}^{\infty} T_{\text{el}} \cos\left(i\theta_e - \varphi_l\right) \tag{6}$$

where T_{tr} denotes the torque ripple, T_{el} and φ_l are the amplitude and phase angular of the harmonic component, and lth denotes the harmonic order.

Remark 1: At the high operating speed of the PMSM, the torque ripple is naturally filtered off by the rotor or load inertias to some extent, and thus, the torque ripple is less than that at the low operating speed [37].

Therefore, the goal of this article is to construct a proper controller such that the dynamic performance of PMSM speed regulation system (2) can be improved in the absence of the torque ripple.

In this article, three practical lemmas are presented as essential instruments for stability analysis.

Lemma 1: If $a > 0$ and $0 < b \leq 1$, then the following inequality holds for $\forall x_1 \in R^n,\ x_2 \in R^n$, $\left|\lfloor x_1 \rceil^{ab} - \lfloor x_2 \rceil^{ab}\right| \leq 2^{1-b}\left|\lfloor x_1 \rceil^{a} - \lfloor x_2 \rceil^{a}\right|^b$.

Lemma 2: If a, b, and c are positive real numbers, then the following inequality holds for $\forall x_1 \in R^n,\ x_2 \in R^n$, $|x_1|^a |x_2|^b \leq \frac{a}{a+b} c|x_1|^{a+b} + \frac{b}{a+b} c^{-\frac{a}{b}} |x_2|^{a+b}$.

Lemma 3: If the real number $0 < c \leq 1$, then the following inequality holds for $\forall x_i \in R^n$ with $i = 1, \ldots, n$, $(|x_1| + \cdots + |x_n|)^c \leq |x_1|^c + \cdots + |x_n|^c$.

III. Design of ILC-DOB and Composite SOSM Controller

For the design of the speed loop control under the FOC framework of the PMSM, the conventional SMC method provides satisfactory control performance. However, the chattering problem caused by discontinuous high-frequency switching signals is an inherent problem. To this end, the SOSM control method is used in this article. Furthermore, the mismatched term and mismatched disturbance are introduced to decrease the uncertainties in the control channel. Especially, due to the fact that the torque ripple is contained in the mismatched disturbance, the composite SOSM controller together with the ILC-DOB is designed.

A. SOSM System and Assumption

For the speed loop control design of the PMSM, one can set w^* as the reference rotor angular velocity. After that, the speed error is defined as the sliding variable $s_1 = w - w^*$. Taking the derivative of sliding variable s_1 with PMSM system (2) and electromagnetic torque (6) in mind, one has

$$\dot{s}_1 = \frac{3p_n\psi_f}{2J} i_q - \frac{1}{J}\left(T_L + Bw - T_{\text{tr}}\right) = s_2 + \varphi(s_1) + d(t) \tag{7}$$

where $s_2 = \frac{3p_n\psi_f}{2J} i_q$ is a new sliding variable, $\varphi(s_1) = -\frac{B}{J}s_1$ denotes the mismatched term, and $d(t) = -\frac{1}{J}(T_L + Bw^* - T_{tr})$ represents the mismatched disturbance. Among them, $\varphi(s_1)$ and $d(t)$ fulfil the following assumption.

Assumption 1: One can find a positive function $\rho(s_1)$ and a positive constant D such that

$$|\varphi(s_1)| \leq \rho\left(s_1\right)|s_1|^{\frac{1}{2}}, \quad \left|\dot{d}(t)\right| \leq D. \tag{8}$$

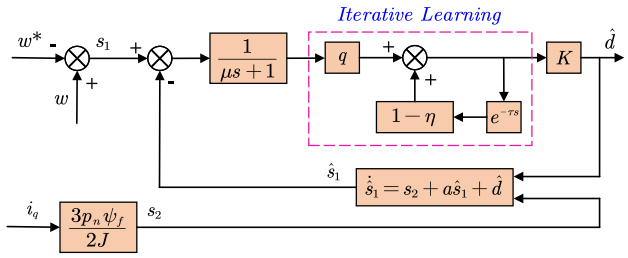

Fig. 1. Block diagram of the ILC-DOB.

Consequently, the sliding variables of the PMSM system are expressed as

$$s_1 = w - w^*, s_2 = \frac{3p_n\psi_f}{2J} i_q. \tag{9}$$

According to the definition of sliding variables (9), PMSM system (2) can be transformed into the following SOSM dynamics with mismatched term and mismatched disturbance:

$$\dot{s}_1 = s_2 + as_1 + d(t), \dot{s}_2 = g(t,x)u \tag{10}$$

where $a = -\frac{B}{J}$, $g(t,x) = \frac{3p_n\psi_f}{2J}$ satisfies $|g(t,x)| \geq g_m$ (g_m is a positive constant), and $u = \dot{i}_q$.

Therefore, the control problem for PMSM speed regulation system (2) is transformed into the stability problem for SOSM dynamics (10).

B. Design of ILC-DOB

In order to estimate the abovementioned mismatched disturbance, a novel ILC-DOB is introduced here [35]. The principle diagram of the ILC-DOB is depicted in Fig. 1.

The design steps are as follows. First, a high-gain DOB is designed to estimate the nonperiodic mismatched disturbance. After that, the high-gain DOB and the iterative learning technique are integrated to construct the ILC-DOB to further estimate the periodic torque ripple.

With the help of SOSM dynamics (10), one can construct a high-gain DOB as

$$\begin{cases} \dot{\hat{s}}_1 = s_2 + a\hat{s}_1 + \hat{d} \\ \hat{d} = K\left(s_1 - \hat{s}_1\right) \end{cases} \tag{11}$$

where $\hat{s}_1, \hat{d}$ represent the estimated values of sliding variable and mismatched disturbance, respectively, and K denotes a positive constant. For convenience of expression, d is used to represent $d(t)$ in the following.

Lemma 4: If the DOB is designed as (11) and the constant gain K is chosen big enough, the observed value $\hat{d}$ will converge to the mismatched disturbance d.

Proof: The proof of Lemma 4 is similar to that of [35, Th. 1]. For simplicity, the proof is omitted here. ■

It is worth noting that d contains periodically varying torque ripple T_{tr}, which cannot be accurately estimated by the time-varying high-gain DOB (11). To suppress the periodic torque ripple, the ILC is applied to the high-gain DOB, which is a data-based error correction algorithm that enhances the suppression capability of the system for the periodic disturbance by learning error information from the previous iteration. The current-iterative learning algorithm [36] is formulated as

$$u_j(t) = (1-\eta)\, u_{j-1}(t) + qe_j(t) \tag{12}$$

where $u_j(t)$ represents the learning term result of jth iteration that is stored in the memory for the next iteration, j denotes the iterative number, $e_j(t)$ denotes the error signal of the jth iteration, η denotes the forgetting factor that is able to attenuate the accumulated effect of aperiodic disturbances, and q denotes the learning gain that influences the tracking accuracy and convergence rate of the ILC.

By combining high-gain DOB (11) with ILC (12), the ILC-DOB is constructed as follows:

$$\begin{cases} \dot{\hat{s}}_{1j} = s_{2j} + a\hat{s}_{1j} + \hat{d}_j \\ e_j = (1-\eta)\, e_{j-1} + q\left(s_{1j} - \hat{s}_{1j}\right) \\ \hat{d}_j = Ke_j \end{cases} \tag{13}$$

where s_{1j} and $\hat{s}_{1j}$ are sliding variable s_1 and estimated sliding variable s_1 of jth iteration, s_{2j} and $\hat{d}_j$ are sliding variable s_2 and estimated disturbance of jth iteration, e_j and e_{j-1} denote the estimated error of sliding variable s_1 of the jth and $(j-1)$th iteration, separately. It should be noted that the iterative cycle T (i.e., the time interval between e_j and e_{j-1}) is chosen as the fundamental period of torque ripple, which is expressed as $T = \frac{2\pi}{p_n w}$.

Lemma 5: For SOSM dynamics (10), if the ILC-DOB is designed as (13), the observed value $\hat{d}_j$ will converge to the disturbance d_j.

Proof: The proof is performed on the iterative domain, which is the discrete form. One should first define a Lyapunov function E_j at jth iteration as

$$E_j = V_{1,j} + V_{2,j} \tag{14}$$

where $V_{1,j} = \frac{1}{2qK}\int_0^t D_j^T D_j d\tau$, $D_j = d_j - \hat{d}_j$, $V_{2,j} = \frac{1}{2}(s_{1j} - \hat{s}_{1j})^2$.

Then, the difference of $V_{1,j}$ between two sequent iterations $\Delta V_{1,j} = V_{1,j} - V_{1,j-1}$ is expressed as follows:

$$\begin{aligned} \Delta V_{1,j} &= \frac{1}{2qK}\int_0^t \left(D_j^T D_j - D_{j-1}^T D_{j-1}\right) d\tau \\ &= \frac{1}{2qK}\int_0^t \left(\hat{d}_{j-1} - \hat{d}_j\right)\left[2\left(d_j - \hat{d}_j\right) + \hat{d}_j - \hat{d}_{j-1}\right] d\tau \\ &= -\int_0^t D_j\left(s_{1j} - \hat{s}_{1j}\right) d\tau + \frac{\eta}{q}\int_0^t D_j e_{j-1} d\tau \\ &\quad - \frac{1}{2qK}\int_0^t \left(\hat{d}_j - \hat{d}_{j-1}\right)^2 d\tau. \end{aligned} \tag{15}$$

The difference of $V_{2,j}$ between two sequent iterations $\Delta V_{2,j} = V_{2,j} - V_{2,j-1}$ is expressed as follows:

$$\begin{aligned} \Delta V_{2,j} &= \frac{1}{2}\left(s_{1j} - \hat{s}_{1j}\right)^2 - V_{2,j-1} \\ &= \int_0^t \left(s_{1j} - \hat{s}_{1j}\right)\left[a\left(s_{1j} - \hat{s}_{1j}\right) + D_j\right] d\tau - V_{2,j-1} \end{aligned}$$

$$= \int_0^t D_j \left(s_{1j} - \hat{s}_{1j}\right) d\tau + a \int_0^t \left(s_{1j} - \hat{s}_{1j}\right)^2 d\tau - \frac{1}{2}\left(s_{1(j-1)} - \hat{s}_{1(j-1)}\right)^2. \tag{16}$$

Thus, one can obtain

$$\begin{aligned}\Delta E_j &= \Delta V_{1,j} + \Delta V_{2,j} \\ &= -\frac{1}{2qK}\int_0^t \left(\hat{d}_j - \hat{d}_{j-1}\right)^2 d\tau - \frac{1}{2}\left(s_{1(j-1)} - \hat{s}_{1(j-1)}\right)^2 \\ &\quad + a\int_0^t \left(s_{1j} - \hat{s}_{1j}\right)^2 d\tau + \frac{\eta}{q}\int_0^t D_j e_{j-1} d\tau. \end{aligned} \tag{17}$$

Considering that $a = -\frac{B}{J} < 0$, and $\frac{\eta}{q}$ is relatively small, (17) can be rewritten as

$$\Delta E_j \le 0 \tag{18}$$

which is negative definite, this implies that the observed error of disturbance d_j will converge to zero asymptotically. ■

Remark 2: Regarding the selection of the control gain K, increasing K will reduce the observation error and phase lag, while the interference of high-frequency noise to the system will increase, which in turn damages the control performance [35]. Therefore, the principle of choosing K is to raise K beginning with a small constant, until the balance between estimation accuracy and noise is satisfied. Considering the selection of the forgetting factor η, the smaller it is, the better the suppressed effect of the ILC-DOB for periodic torque ripple, but the cumulative impact of aperiodic disturbance is greater, so the forgetting factor η is not suitable for taking too small. For the learning gain q, a larger learning gain will accelerate the convergence speed of the ILC, while it will reduce the error convergence accuracy of the ILC.

C. Design of the Composite SOSM Controller

According to Lemma 5, the estimated disturbance $\hat{d}_j$ will converge to d_j, that is, SOSM dynamics (10) can be further rewritten as

$$\dot{s}_1 = s_2 + as_1 + \hat{d}_j, \dot{s}_2 = g(t,x)u. \tag{19}$$

Obviously, if a controller can be designed to stabilize SOSM dynamics (19), it can also stabilize SOSM dynamics (10). On this basis, the following theorem can be given.

Theorem 1: For SOSM dynamics (19) satisfying Assumption 1, there is a positive constant $\alpha \ge \beta^{\frac{1}{2}}$, which enables the following composite SOSM controller u to realize SOSM $s_1 = \dot{s}_1 = 0$ in finite time

$$u = -\alpha \cdot \operatorname{sign}\left(\lfloor s_2 + \hat{d}_j \rceil^2 + \beta s_1\right). \tag{20}$$

Proof: With the help of the adding a power integrator method, the proof is carried out in two steps.

Step 1: Select the Lyapunov candidate function as

$$V_1(s_1) = \frac{2}{5}|s_1|^{\frac{5}{2}}.$$

According to Assumption 1, the derivative of $V_1(s_1)$ along SOSM dynamics (19) can be obtained as

$$\begin{aligned}\frac{d}{dt}V_1(s_1) &= \lfloor s_1 \rceil^{\frac{3}{2}}\left(s_2 + as_1 + \hat{d}_j\right) \\ &\le \lfloor s_1 \rceil^{\frac{3}{2}}(s_2 - s_2^*) + \lfloor s_1 \rceil^{\frac{3}{2}} s_2^* \\ &\quad + \rho(s_1)\lfloor s_1 \rceil^2 + \lfloor s_1 \rceil^{\frac{3}{2}}\hat{d}_j \end{aligned} \tag{21}$$

where s_2^* is a virtual controller designed as

$$s_2^* = -\beta^{\frac{1}{2}}\lfloor s_1 \rceil^{\frac{1}{2}} - \hat{d}_j \tag{22}$$

with $\beta^{\frac{1}{2}} \ge \rho(s_1) + \beta_0$, $\beta_0 > 0$. Substituting virtual controller (22) into inequality (21) yields

$$\frac{d}{dt}V_1(s_1) \le -\beta_0 s_1^2 + \lfloor s_1 \rceil^{\frac{3}{2}}(s_2 - s_2^*). \tag{23}$$

Step 2: Choose the Lyapunov function as

$$V_2(s_1, \bar{s}_2) = V_1(s_1) + W(s_1, \bar{s}_2)$$

where $W(s_1, \bar{s}_2) = \int_{\bar{s}_2^*}^{\bar{s}_2} \lfloor \lfloor k \rceil^2 - \lfloor \bar{s}_2^* \rceil^2 \rceil^2 dk$, $\bar{s}_2 = s_2 + \hat{d}_j$ and $\bar{s}_2^* = s_2^* + \hat{d}_j$. Taking the derivative of $V_2(s_1, \bar{s}_2)$ along SOSM dynamics (19) can be obtained as

$$\begin{aligned}\frac{d}{dt}V_2(s_1, \bar{s}_2) &= \frac{d}{dt}V_1(s_1) + \frac{\partial W(s_1, \bar{s}_2)}{\partial s_1}\dot{s}_1 + \frac{\partial W(s_1, \bar{s}_2)}{\partial \bar{s}_2}\dot{\bar{s}}_2 \\ &\le -\beta_0 s_1^2 + \lfloor s_1 \rceil^{\frac{3}{2}}(s_2 - s_2^*) \\ &\quad + \frac{\partial W(s_1, \bar{s}_2)}{\partial s_1}\dot{s}_1 + \lfloor \zeta \rceil^2 \dot{\bar{s}}_2 \end{aligned} \tag{24}$$

where $\zeta = \lfloor \bar{s}_2 \rceil^2 - \lfloor \bar{s}_2^* \rceil^2$. Next, the terms on the right-hand side of inequality (24) need to be estimated.

First of all, notice that $|s_2 - s_2^*| = |\bar{s}_2 - \bar{s}_2^*| = |\lfloor \bar{s}_2 \rceil^{2\times\frac{1}{2}} - \lfloor \bar{s}_2^* \rceil^{2\times\frac{1}{2}}|$. By using Lemma 1, it is obtained that

$$\lfloor s_1 \rceil^{\frac{3}{2}}(s_2 - s_2^*) \le 2^{\frac{1}{2}}|s_1|^{\frac{3}{2}}|\zeta|^{\frac{1}{2}}. \tag{25}$$

Then, applying Lemma 2 to (25) produces

$$\begin{aligned}\lfloor s_1 \rceil^{\frac{3}{2}}(s_2 - s_2^*) &\le 2^{\frac{1}{2}}\left(\frac{3}{4}cs_1^2 + \frac{1}{4}c^{-3}\zeta^2\right) \\ &\le \frac{1}{4}\beta_0 s_1^2 + \gamma_1 \zeta^2 \end{aligned} \tag{26}$$

where $2^{\frac{1}{2}}\frac{3}{4}c = \frac{1}{4}\beta_0$, $c = \frac{\beta_0}{3\cdot 2^{\frac{1}{2}}}$, and $\gamma_1 = 2^{\frac{1}{2}}\frac{1}{4}(\frac{3\cdot 2^{\frac{1}{2}}}{\beta_0})^3$.

Second, it can be calculated that

$$\left|\frac{\partial W(s_1, \bar{s}_2)}{\partial s_1}\dot{s}_1\right| \le 2|\bar{s}_2 - \bar{s}_2^*||\zeta|\left|\frac{\partial \lfloor \bar{s}_2^* \rceil^2}{\partial s_1}\dot{s}_1\right|. \tag{27}$$

Applying Lemma 1 to (27) can obtain

$$\left|\frac{\partial W(s_1, \bar{s}_2)}{\partial s_1}\dot{s}_1\right| \le 2^{\frac{3}{2}}|\zeta|^{\frac{3}{2}}\left|\frac{\partial \lfloor \bar{s}_2^* \rceil^2}{\partial s_1}\dot{s}_1\right|. \tag{28}$$

Due to $\bar{s}_2^* = s_2^* + \hat{d}_j$, putting virtual controller (22) into $\bar{s}_2^*$ obtains

$$\frac{\partial \lfloor \bar{s}_2^* \rceil^2}{\partial s_1} = -\beta. \tag{29}$$

In addition, with $\dot{s}_1 = \bar{s}_2 + as_1$ in mind, it can be obtained by using Lemma 3 and Assumption 1 that

$$|\bar{s}_2 + as_1| \leq |\zeta|^{\frac{1}{2}} + \beta^{\frac{1}{2}} |s_1|^{\frac{1}{2}} + \rho(s_1) |s_1|^{\frac{1}{2}}. \quad (30)$$

Integrating (29) and (30) results in

$$\left| \frac{\partial \lfloor \bar{s}_2^* \rceil^2}{\partial s_1} \dot{s}_1 \right| \leq \gamma_2(s_1) |s_1|^{\frac{1}{2}} + \beta |\zeta|^{\frac{1}{2}} \quad (31)$$

where $\gamma_2(s_1) = \beta^{\frac{3}{2}} + \beta\rho(s_1)$. Plugging (31) into (28) obtains

$$\left| \frac{\partial W(s_1, \bar{s}_2)}{\partial s_1} \dot{s}_1 \right| \leq 2^{\frac{3}{2}} |\zeta|^{\frac{3}{2}} \cdot \gamma_2(s_1) |s_1|^{\frac{1}{2}} + 2^{\frac{3}{2}} \beta |\zeta|^2. \quad (32)$$

Using Lemma 2 again, (32) can be further expanded as

$$\left| \frac{\partial W(s_1, \bar{s}_2)}{\partial s_1} \dot{s}_1 \right| \leq 2^{\frac{3}{2}} \gamma_2(s_1) \cdot \frac{1}{4} c_1^{-3} s_1^2 + 2^{\frac{3}{2}} \gamma_2(s_1) \cdot \frac{3}{4} c_1 \zeta^2 + 2^{\frac{3}{2}} \beta \zeta^2. \quad (33)$$

Let $2^{\frac{3}{2}} \gamma_2(s_1) \cdot \frac{1}{4} c_1^{-3} = \frac{1}{4}\beta_0$, and $\gamma_3(s_1) = 2^{\frac{3}{2}} \gamma_2(s_1) \cdot \frac{3}{4} c_1 + 2^{\frac{3}{2}} \beta$, then (33) can be rewritten as

$$\left| \frac{\partial W(s_1, \bar{s}_2)}{\partial s_1} \dot{s}_1 \right| \leq \frac{1}{4} \beta_0 s_1^2 + \gamma_3(s_1) \zeta^2. \quad (34)$$

Finally, substituting (26) and (34) into (24) yields

$$\frac{d}{dt} V_2(s_1, \bar{s}_2) \leq -\frac{1}{2} \beta_0 s_1^2 + \gamma_1 \zeta^2 + \gamma_3(s_1) \zeta^2 + \lfloor \zeta \rceil^2 \left[g(t,x) u + \dot{d}_j \right]. \quad (35)$$

By Assumption 1, it is obvious that $|\dot{d}_j(t)| \leq D$. Therefore, the controller u can be designed as

$$u = -\alpha \cdot \mathrm{sign}(\zeta) \quad (36)$$

where $\alpha \geq \frac{D + \gamma_1 + \gamma_3(s_1) + \frac{\beta_0}{2}}{g_m}$. Putting controller (36) into (35) yields

$$\frac{d}{dt} V_2(s_1, \bar{s}_2) \leq -\frac{\beta_0}{2} \left(s_1^2 + \zeta^2 \right). \quad (37)$$

With the help of Lemma 3, one can get

$$\left(\left| s_1^{\frac{5}{2}} \right| + \left| \zeta^{\frac{5}{2}} \right| \right)^{\frac{4}{5}} \leq \left| s_1^{\frac{5}{2}} \right|^{\frac{4}{5}} + \left| \zeta^{\frac{5}{2}} \right|^{\frac{4}{5}} = s_1^2 + \zeta^2. \quad (38)$$

Combining (37) with (38) yields

$$\frac{d}{dt} V_2(s_1, \bar{s}_2) \leq -\frac{\beta_0}{2} \left(\left| s_1^{\frac{5}{2}} \right| + \left| \zeta^{\frac{5}{2}} \right| \right)^{\frac{4}{5}}. \quad (39)$$

According to the definition of function $W(s_1, \bar{s}_2)$, it follows that

$$\int_{\bar{s}_2^*}^{\bar{s}_2} \lfloor \lfloor k \rceil^2 - \lfloor \bar{s}_2^* \rceil^2 \rceil^2 dk \leq 2^{\frac{1}{2}} |\zeta|^{\frac{5}{2}}. \quad (40)$$

Thus, integrating the definition of function $V_1(s_1)$ and (40) yields

$$V_2(s_1, \bar{s}_2) \leq 2 \left(|s_1|^{\frac{5}{2}} + |\zeta|^{\frac{5}{2}} \right). \quad (41)$$

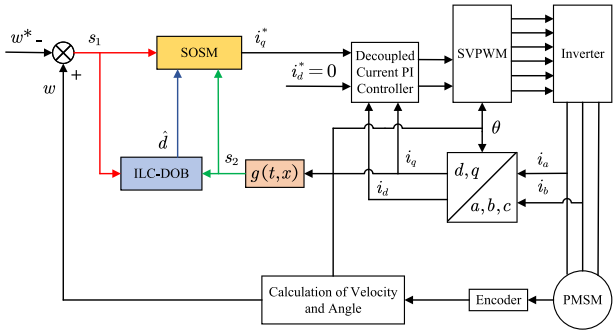

Fig. 2. Control diagram of PMSM system.

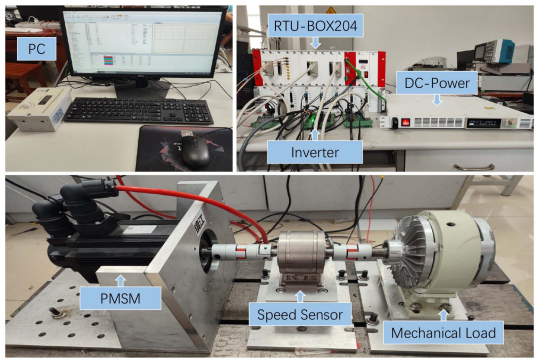

Fig. 3. Experimental platform.

Plugging (41) into (39) results in

$$\frac{d}{dt} V_2(s_1, \bar{s}_2) \leq -2^{-\frac{9}{5}} \beta_0 \cdot V_2^{\frac{4}{5}}(s_1, \bar{s}_2). \quad (42)$$

Obviously, controller (36) is the same as composite SOSM controller (20). According to the finite-time Lyapunov theory [29], SOSM dynamics (19) can be finite-time stabilized under controller (20). That means SOSM dynamics (10) also be finite-time stabilized under controller (20). ■

Remark 3: It can be seen that the parameter β is related to almost all other parameters, because we have employed a backstepping-like method to deal with the control law design for the considered system. Moreover, the control parameters will increase significantly with the size of the system due to the nature of the backstepping method. Therefore, according to the virtual controller (22), a very small β and a proper α can be chosen first, so that the sliding variable s_1 can be driven to zero. On this basis, the best performance of the closed-loop system can be obtained by turning the parameter β from small to large.

Accordingly, the principle diagram of the PMSM system under SOSM controller with ILC-DOB (20) is depicted in Fig. 2.

IV. Experimental Results and Discussions

For the purpose of verifying the performance of the proposed composite SOSM control method, the comparative experiment is carried out on the 1.5 kW three-phase PMSM experimental platform, which is shown in Fig. 3. The platform adopts a three-phase motor with the model of 130ST-M10015 and an

TABLE I
KEY PARAMETERS OF THE PMSM PLATFORM

Parameter	Unit	Value
Rated speed S_r	r/min	1500
Rated phase current I_r	A	6
Stator inductance L_s	mH	4.37
Number of poles p_n	-	4
Rated power P_r	kW	1.5
Flux linkage ψ_f	wb	0.142
Rated torque T_r	N/m	10
Stator resistance R_s	Ω	1.5
Moment of inertia J	$\mathrm{kg/m^2}$	0.00194

RTU-BOX204 real-time digital controller. The values of the parameters are shown in Table I.

To have a clearer comparison, the conventional SMC, the SOSM control, the SOSM control with high-gain DOB, and the proposed SOSM control with ILC-DOB are applied to the PMSM system. They are experimented with and analyzed under different operating conditions (i.e., no-load startup, load torque variations).

By the first-order sliding-mode concept, the conventional integral sliding-mode surface is first selected as

$$s = s_1 + c\int_0^t s_1 dt. \tag{43}$$

On this basis, the first-order sliding mode (SM) control law [20] is designed as

$$u_1 = -\frac{2J}{3p_n\psi_f}\left(-\frac{B}{J}+c\right)s_1 - k_1\cdot\mathrm{sign}(s), k_1>0. \tag{44}$$

According to the sliding variables (9) and controller (20), the SOSM controller is designed as

$$u_2 = -\alpha_2\cdot\mathrm{sign}\left(\lfloor\dot{s}_1\rceil^2+\beta_2 s_1\right), \alpha_2>0. \tag{45}$$

And from the high-gain DOB (11) and controller (20), the SOSM controller with high-gain DOB is designed as

$$u_3 = -\alpha_3\cdot\mathrm{sign}\left(\lfloor s_2+\hat{d}\rceil^2+\beta_3 s_1\right), \alpha_3>0. \tag{46}$$

Considering the reasonableness of the experimental comparison, all the abovementioned algorithms use PI control with the same parameters in the current loop (i.e., proportional gain $K_p = 1.5$, integral gain $K_i = 4.2$).

A. PMSM Startup and Antidisturbance Property

This section analyzes the property of startup and antidisturbance, and the ability to weaken the chattering problem under SM controller (44), SOSM controller (45), and SOSM controller with ILC-DOB (20). To have a fair comparison, the parameters of these controllers are arbitrarily taken to get the best performance. In this case, the parameters of SM controller (44) are selected as $c = 700$, $k_1 = 800$. The parameters of SOSM controller (45) are selected as $\alpha_2 = 300$, $\beta_2 = 540$, and the parameters of SOSM controller with ILC-DOB (20) are chosen as $\alpha = 230$, $\beta = 540$, $K = 60$, $\eta = 0.16$, $q = 0.8$.

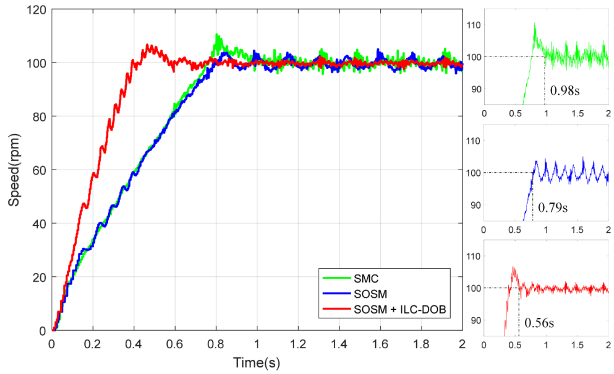

Fig. 4. Speed responses of no-load startup under the SMC, the SOSM, and the SOSM with ILC-DOB.

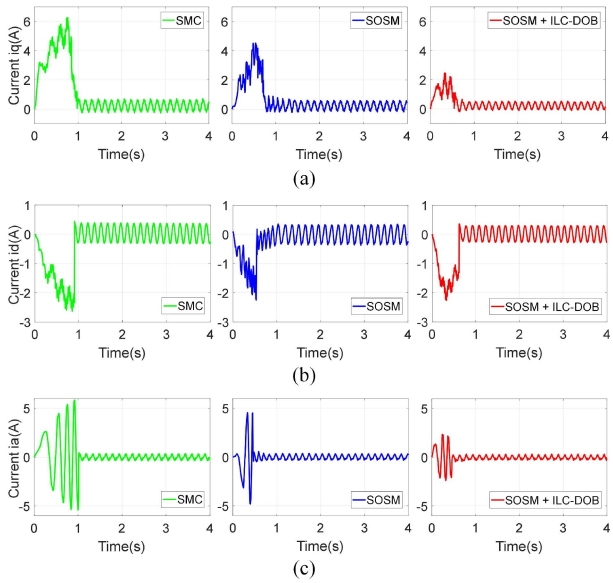

Fig. 5. Current responses of no-load startup under the SMC, the SOSM, and the SOSM with ILC-DOB. (a) i_q. (b) i_d. (c) i_a.

During the startup phase of the PMSM, the motor speed reference is set to 100 r/min without additional load torque. The startup performance under the three controllers is shown in Figs. 4 and 5, from which it can be concluded that the speed response curve under SM controller (44) not only has the largest settling time but also has a large overshoot. It can also be observed that there is no overshoot during startup under SOSM controller (45). In addition, under SOSM controller with ILC-DOB (20), the speed response curve has a slight overshoot but its settling time is significantly less than that under SM controller (44) and SOSM controller (45), and the peak of the q-axis current is relatively small. Consequently, the SOSM controller with ILC-DOB (20) shows the best startup performance.

In the meantime, the disturbance rejection property under the three controllers in the cases of sudden load and sudden unload are depicted in Figs. 6–9. The load is added suddenly at $t = 7.45$ s and removed at $t = 12.4$ s. It can be summarized from Figs. 6 and 8 that the PMSM system under SOSM controller with ILC-DOB (20) has lower speed fluctuation and shorter settling

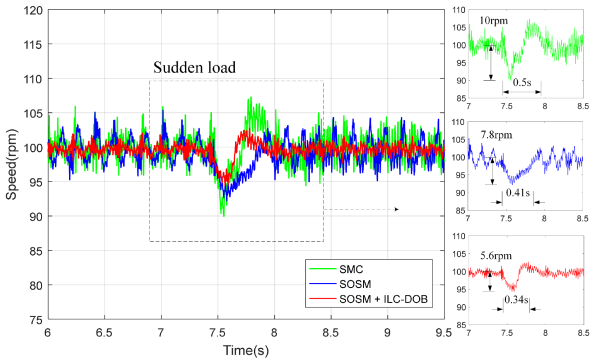

Fig. 6. Speed responses with a sudden load under the SMC, the SOSM, and the SOSM with ILC-DOB.

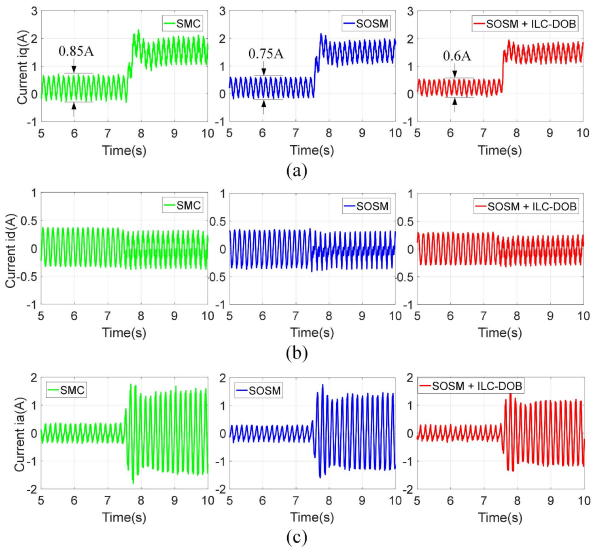

Fig. 7. Current responses of sudden load under the SMC, the SOSM, and the SOSM with ILC-DOB. (a) i_q. (b) i_d. (c) i_a.

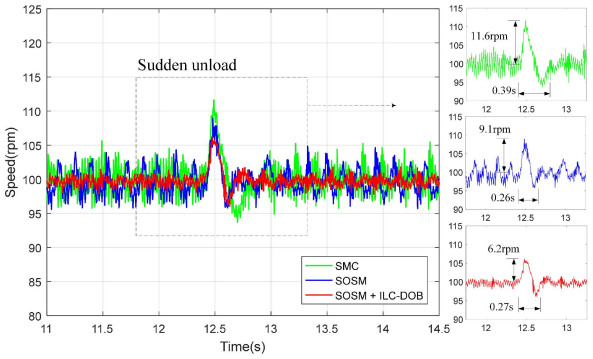

Fig. 8. Speed responses with a sudden unload under the SMC, the SOSM, and the SOSM with ILC-DOB.

time than that under SM controller (44) and SOSM controller (45) during load torque variations. Furthermore, it can be noticed from Fig. 7(a) that the ripple of the q-axis current under SOSM controller with ILC-DOB (20) is decreased due to the lower control gain, which implies that the chattering problem is weakened. Combining the abovementioned experiment results,

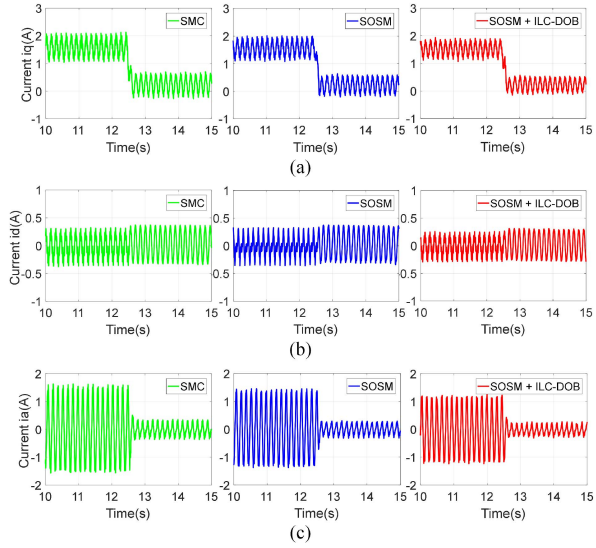

Fig. 9. Current responses of sudden unload under the SMC, the SOSM, and the SOSM with ILC-DOB. (a) i_q. (b) i_d. (c) i_a.

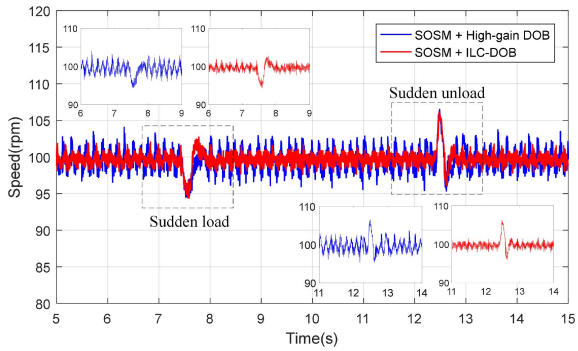

Fig. 10. Speed responses of load torque variations under the SOSM with ILC-DOB and the SOSM with high-gain DOB.

several critical property indicators for the three controllers are presented in Table II.

As shown in Table II, although the switching gain of SOSM controller with ILC-DOB (20) is smaller than that of SM controller (44) and SOSM controller (45), the startup performance and disturbance rejection property under SOSM controller with ILC-DOB (20) is still better than them.

B. Torque Ripple Suppression Analysis

For the purpose of verifying the performance of the ILC-DOB in reducing torque ripple, the SOSM control with ILC-DOB and the SOSM control with high-gain DOB are used to control the motor for experiments at two reference speeds of 100 r/min and 60 r/min. The parameters of SOSM controller with ILC-DOB (20) are the same as before, and the parameters of SOSM controller with high-gain DOB (46) are chosen as $\alpha_3 = 230$, $\beta_3 = 540$, $K = 60$.

Due to the usage of iterative learning, it can be observed from Figs. 10 and 12(a) that the speed fluctuation under SOSM controller with ILC-DOB (20) is about 3.4 r/min, which is lower

TABLE II
PROPERTY INDICATORS FOR THE SMC, THE SOSM, AND THE SOSM WITH ILC-DOB CONTROLLERS

Control algorithm	Startup		Sudden load		Sudden unload	
	Overshoot(%)	Settling time(s)	Speed fluctuation (r/min)	Settling time(s)	Speed fluctuation (r/min)	Settling time(s)
SMC	10.1	0.98	10.0	0.50	11.6	0.39
SOSM	None	0.79	7.8	0.41	9.1	0.26
SOSM + ILC-DOB	5.3	0.56	5.6	0.34	6.2	0.27

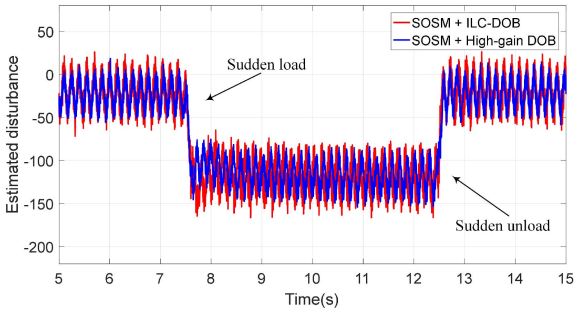

Fig. 11. Estimated values under the ILC-DOB and high-gain DOB.

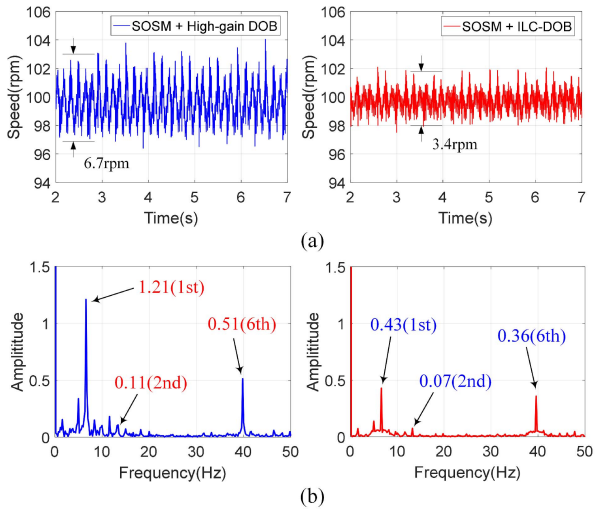

Fig. 12. Experimental results of the SOSM with ILC-DOB and the SOSM with high-gain DOB controllers at 100 r/min. (a) Speed responses. (b) Harmonic amplitudes in speed.

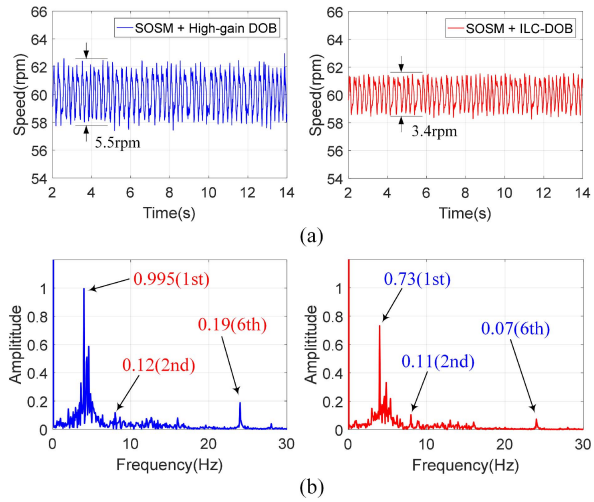

Fig. 13. Experimental results of the SOSM with ILC-DOB and the SOSM with high-gain DOB controllers at 60 r/min. (a) Speed responses. (b) Harmonic amplitudes in speed.

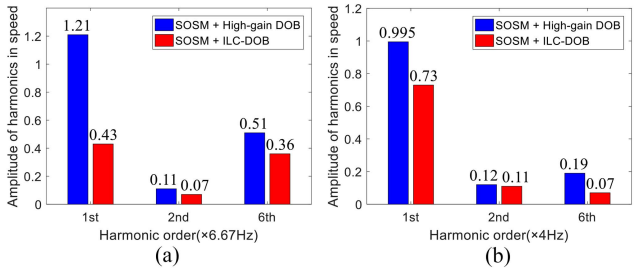

Fig. 14. Comparison results of the harmonic amplitudes under the SOSM with ILC-DOB and the SOSM with high-gain DOB. (a) At 100 r/min. (b) At 60 r/min.

than 6.7 r/min under SOSM controller with high-gain DOB (46). Although the disturbance rejection property of the ILC-DOB is slightly lower than that of the high-gain DOB during load torque variations, this difference is within the acceptable range. Meanwhile, Fig. 11 shows the estimations of the lumped disturbance under the ILC-DOB and the high-gain DOB. It is obvious that the ILC-DOB can track periodic disturbances more accurately. The aforementioned experimental conclusions reveal that the proposed SOSM controller with ILC-DOB (20) not only has satisfying robustness but also can minimize the speed ripple.

To further analyze the ability of the ILC-DOB in suppressing the torque ripple, the speed harmonic components under SOSM controller with high-gain DOB (46) and SOSM controller with ILC-DOB (20) are obtained by using the fast Fourier transformation. At the reference speed of 100 r/min, the steady-state speed data from 2 to 7 s are analyzed in Fig. 12. It can be clearly observed from Figs. 12(b) and 14(a) that the first, second, and sixth harmonic components under SOSM with high-gain DOB (46) are 1.21, 0.11, and 0.51 r/min, respectively. After the combination of ILC-DOB and SOSM, the first, second, and sixth harmonic components reduce to 0.43, 0.07, and 0.36 r/min, separately. According to frequency domain analysis, the main harmonic components of the torque ripple can be effectively suppressed by using iterative learning.

Next, for more comprehensive verification, the steady-state speed data from 2 to 14 s are analyzed at the reference speed of 60 r/min. It can be seen from Fig. 13(a) that the speed ripple under SOSM controller with high-gain DOB (46) and SOSM controller with ILC-DOB (20) are about 5.5 and 3.4 r/min, respectively. Furthermore, as depicted in Figs. 13(b) and 14(b), the first, second, and sixth harmonic components are significantly reduced at 60 r/min by using iterative learning.

Through the aforementioned experimental data and analysis, it is verified that the proposed SOSM controller with ILC-DOB possesses good dynamic performance and torque ripple suppression ability for the PMSM system.

V. Conclusion

In this article, a composite SOSM control algorithm combined with a novel ILC-DOB scheme has been presented and applied to the surface-mounted PMSM. The composite SOSM control algorithm can handle the mismatched disturbance to improve the robustness of the system so that the chattering problem can be weakened by selecting a smaller switching gain. Furthermore, the proposed ILC-DOB is able to accurately estimate the periodic torque ripple of the PMSM and minimize it. The proposed composite SOSM control algorithm is validated by conducting experiments on the motor platform under different operating conditions, and the experimental results demonstrate the effectiveness of the proposed algorithm. Our future work will be devoted to the design of ILC applied in the current loop for minimizing the torque ripple caused by current measurement errors. Moreover, using adaptive techniques into the PMSM system to address parameter changes dynamically is a promising research direction.

References

[1] Y. Zhao, Z. Wang, D. Luo, C. Chen, B. Ji, and G. Li, "Multitimescale thermal network model of power devices based on POD algorithm," *IEEE Trans. Power Electron.*, vol. 39, no. 4, pp. 3906–3924, Apr. 2024.

[2] C. Ren et al., "Improving dv/dt immunity of reverse blocking IGCT for hybrid line-commutated converter," *IEEE Trans. Power Electron.*, vol. 39, no. 4, pp. 4001–4005, Apr. 2024.

[3] Y. Dai, L. Zhang, D. Xu, Q. Chen, and X. Yan, "Anti-disturbance cooperative fuzzy tracking control of multi-PMSMs low-speed urban rail traction systems," *IEEE Trans. Transport. Electrific.*, vol. 8, no. 1, pp. 1040–1052, Mar. 2022.

[4] C. Sun, D. Sun, W. Chen, and H. Nian, "Improved model predictive control with new cost function for hybrid-inverter open-winding PMSM system based on energy storage model," *IEEE Trans. Power Electron.*, vol. 36, no. 9, pp. 10705–10715, Sep. 2021.

[5] Y. Fan, J. Chen, Q. Zhang, and M. Cheng, "An improved inertia disturbance suppression method for PMSM based on disturbance observer and two-degree-of-freedom PI controller," *IEEE Trans. Power Electron.*, vol. 38, no. 3, pp. 3590–3599, Mar. 2023.

[6] M. S. Mubarok, T.-H. Liu, S. A. Davari, and J. Rodriguez, "Constrained predictive controllers for high-performance sensorless IPMSM drive systems with full-range speed operations," *IEEE Trans. Power Electron.*, vol. 39, no. 4, pp. 4612–4623, Apr. 2024.

[7] P. Luo, Z. Yin, Z. Zhang, Y. Zhang, P. Zhang, and J. Liu, "Diversified diagnosis strategy for PMSM inter-turn short-circuit fault via novel sliding mode observer," *IEEE Trans. Power Electron.*, vol. 39, no. 4, pp. 4149–4159, Apr. 2024.

[8] F. Aghili, "Optimal feedback linearization control of interior PM synchronous motors subject to time-varying operation conditions minimizing power loss," *IEEE Trans. Ind. Electron.*, vol. 65, no. 7, pp. 5414–5421, Jul. 2018.

[9] Y. S. Choi, H. H. Choi, and J. W. Jung, "Feedback linearization direct torque control with reduced torque and flux ripples for IPMSM drives," *IEEE Trans. Power Electron.*, vol. 31, no. 5, pp. 3728–3737, May 2016.

[10] L. Rovere, A. Formentini, and P. Zanchetta, "FPGA implementation of a novel oversampling deadbeat controller for PMSM drives," *IEEE Trans. Ind. Electron.*, vol. 66, no. 5, pp. 3731–3741, May 2019.

[11] G. Scarcella, G. Scelba, M. Pulvirenti, and R. D. Lorenz, "Fault-tolerant capability of deadbeat-direct torque and flux control for three-phase PMSM drives," *IEEE Trans. Ind. Appl.*, vol. 53, no. 6, pp. 5496–5508, Nov./Dec. 2017.

[12] Y. Zhang, D. Xu, J. Liu, S. Gao, and W. Xu, "Performance improvement of model-predictive current control of permanent magnet synchronous motor drives," *IEEE Trans. Ind. Appl.*, vol. 53, no. 4, pp. 3683–3695, Jul./Aug. 2017.

[13] X. Zhang, C. Zhang, C. Xu, and S. Fan, "Multimode model predictive control for PMSM drive system," *IEEE Trans. Transport. Electrific.*, vol. 9, no. 1, pp. 667–677, Mar. 2023.

[14] S. Suganthi and R. Karpagam, "Dynamic performance improvement of PMSM drive using fuzzy-based adaptive control strategy for EV applications," *J. Power Electron.*, vol. 23, no. 3, pp. 510–521, Feb. 2023.

[15] H. Li, S. Wang, Y. Xie, S. Zheng, and P. Shi, "Virtual reference-based fuzzy non-cascade speed control for PMSM systems with unmatched disturbances and current constraints," *IEEE Trans. Fuzzy Syst.*, vol. 31, no. 12, pp. 4249–4261, Dec. 2023.

[16] P. Pietrzak, M. Wolkiewicz, and T. Orlowska-Kowalska, "PMSM stator winding fault detection and classification based on bispectrum analysis and convolutional neural network," *IEEE Trans. Ind. Electron.*, vol. 70, no. 5, pp. 5192–5202, May 2023.

[17] Q. Hou and S. Ding, "Finite-time extended state observer based super-twisting sliding mode controller for PMSM drives with inertia identification," *IEEE Trans. Transport. Electrific.*, vol. 8, no. 2, pp. 1918–1929, Jun. 2022.

[18] L. He, F. Wang, and D. Ke, "FPGA-based sliding-mode predictive control for PMSM speed regulation system using an adaptive ultralocal model," *IEEE Trans. Power Electron.*, vol. 36, no. 5, pp. 5784–5793, May 2021.

[19] A. Levant, "Higher order sliding modes and their application for controlling uncertain processes," Ph.D. Dissertation, Inst. System Stud., USSR Academy of Science, Moscow, Russia, 1987.

[20] L. Ma, C. Cheng, J. Guo, B. Shi, S. Ding, and K. Mei, "Direct yaw-moment control of electric vehicles based on adaptive sliding mode," *Math. Biosciences Eng.*, vol. 20, no. 7, pp. 13334–13355, Jun. 2023.

[21] S. Ding, Q. Hou, and H. Wang, "Disturbance-observer-based second-order sliding mode controller for speed control of PMSM drives," *IEEE Trans. Energy Convers.*, vol. 38, no. 1, pp. 100–110, Mar. 2023.

[22] J. Sun, Q. Li, S. Ding, G. Xing, and L. Chen, "Fixed-time generalized super-twisting control for path tracking of autonomous agricultural vehicles considering wheel slipping," *Comput. Electron. Agriculture*, vol. 213, Oct. 2023, Art. no. 108231.

[23] A. Ferrara and G. P. Incremona, "Design of an integral suboptimal second-order sliding mode controller for the robust motion control of robot manipulators," *IEEE Trans. Control Syst. Technol.*, vol. 23, no. 6, pp. 2316–2325, Nov. 2015.

[24] W. Yang, S. Ding, and C. Ding, "Fast super-twisting sliding mode control with anti-peaking extended state observer for path-tracking of unmanned agricultural vehicles," *IEEE Trans. Ind. Electron.*, to be published, doi: 10.1109/TIE.2024.3355507.

[25] A. Levant and B. Shustin, "Quasi-continuous MIMO sliding-mode control," *IEEE Trans. Autom. Control*, vol. 63, no. 9, pp. 3068–3074, Sep. 2018.

[26] L. Ma, K. Mei, S. Ding, and T. Pan, "Design of adaptive fuzzy fixed-time HOSM controller subject to asymmetric output constraints," *IEEE Trans. Fuzzy Syst.*, vol. 31, no. 9, pp. 2989–2999, Sep. 2023.

[27] C. Qian and W. Lin, "A continuous feedback approach to global strong stabilization of nonlinear systems," *IEEE Trans. Autom. Control*, vol. 46, no. 7, pp. 1061–1079, Jul. 2001.

[28] W. Dou, S. Ding, and X. Yu, "Event-triggered second-order sliding-mode control of uncertain nonlinear systems," *IEEE Trans. Syst., Man, Cybern. Syst.*, vol. 53, no. 11, pp. 7269–7279, Nov. 2023.

[29] W. Dou, S. Ding, and J. H. Park, "Practical event-triggered finite-time second-order sliding mode controller design," *IEEE Trans. Cybern.*, vol. 54, no. 3, pp. 1972–1983, Mar. 2024.

[30] C. Ding, S. Ding, X. Wei, X. Ji, J. Sun, and K. Mei, "Disturbance-observer-based barrier function adaptive sliding mode control for path tracking of autonomous agricultural vehicles with matched-mismatched disturbances," *IEEE Trans. Transport. Electrific.*, to be published, doi: 10.1109/TTE.2023.3333001.

[31] W. Deng and J. Yao, "Extended-state-observer-based adaptive control of electrohydraulic servomechanisms without velocity measurement," *IEEE/ASME Trans. Mechatronics*, vol. 25, no. 3, pp. 1151–1161, Jun. 2020.

[32] F. Kong, C. Ju, Y. Liu, and C. Lei, "Model-based sensorless control of an IPMSM with enhanced robustness against load disturbances based on position and speed estimator using a speed error," *IEEE Trans. Ind. Appl.*, vol. 54, no. 2, pp. 1448–1459, Mar./Apr. 2018.

[33] Y. Zuo, X. Zhu, L. Quan, and C. Zhan, "Active disturbance rejection controller for speed control of electrical drives using phase-locking loop observer," *IEEE Trans. Ind. Electron.*, vol. 66, no. 3, pp. 1748–1759, Mar. 2019.
[34] W. Qian, S. Panda, and J. Xu, "Torque ripple minimization in PM synchronous motors using iterative learning control," *IEEE Trans. Ind. Electron.*, vol. 19, no. 2, pp. 272–279, Mar. 2004.
[35] T. Yang, Y. Deng, H. Li, Z. Sun, H. Cao, and Z. Wei, "Fast integral terminal sliding mode control with a novel disturbance observer based on iterative learning for speed control of PMSM," *ISA Trans.*, vol. 134, pp. 460–471, Aug. 2022.
[36] D. Bristow, M. Tharayil, and A. Alleyne, "A survey of iterative learning control," *IEEE Control Syst. Mag.*, vol. 26, no. 3, pp. 96–114, Jun. 2006.
[37] J. Liu, H. Li, and Y. Deng, "Torque ripple minimization of PMSM based on robust ILC via adaptive sliding mode control," *IEEE Trans. Power Electron.*, vol. 33, no. 4, pp. 3655–3671, Apr. 2018.
[38] S. A. Q. Mohammed, H. H. Choi, and J. W. Jung, "Improved iterative learning direct torque control for torque ripple minimization of surface-mounted permanent magnet synchronous motor drives," *IEEE Trans. Ind. Informat.*, vol. 17, no. 11, pp. 7291–7303, Nov. 2021.
[39] S. Mandra, K. Galkowski, E. Rogers, A. Rauh, and H. Aschemann, "Performance-enhanced robust iterative learning control with experimental application to PMSM position tracking," *IEEE Trans. Control Syst. Technol.*, vol. 27, no. 4, pp. 1813–1819, Jul. 2019.

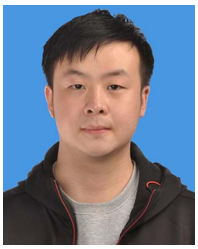

Chang Cheng was born in Hunan, China, in 1998. He is currently working toward the M.S. degree in electronic and information engineering with the School of Electrical and Information Engineering, Jiangsu University, Zhenjiang, China.

His research interests include iterative learning control, sliding-mode control, and their applications.

Lu Liu received the B.E. degree in automation and the Ph.D. degree in control science and engineering from Jiangsu University, Zhenjiang, China, in 2015 and 2020, respectively.

During the graduate studies, he visited Western Sydney University, Sydney, NSW, Australia, from 2018 to 2019. Since February 2021, he has been with the School of Electrical and Information Engineering, Jiangsu University, where he is currently a Lecturer. His research interests include high-order sliding-mode control and intelligent control.

Shihong Ding (Senior Member, IEEE) was born in Anhui, China, in 1983. He received the B.E. degree in mathematics from Anhui Normal University, Wuhu, China, in 2004, and the M.S. and Ph.D. degrees in automatic control from Southeast University, Nanjing, China, in 2007 and 2010, respectively.

During the graduate studies, he visited The University of Texas at San Antonio, San Antonio, TX, USA, from 2008 to 2009. After graduation, he held a Research Fellowship with the University of Western Sydney, Parramatta NSW, Australia, for one year. He also visited Yeungnam University, Gyeongsan, South Korea, from July to August 2018, and RMIT University, Melbourne, VIC, Australia, from 2019 to 2020, respectively. Since 2010, he has been with the School of Electrical and Information Engineering, Jiangsu University, Zhenjiang, China, where he is currently a Full Professor. His research interests include sliding-mode control and motion control.

Dr. Ding is currently a Subject Editor for *Nonlinear Dynamics* and an Associate Editor for *International Journal of Adaptive Control and Signal Processing*.